Relative influence of mechanical and meteorological factors on avalanche release depth distributions: An application to French Alps

J. Gaume,[1] G. Chambon,[1] N. Eckert,[1] and M. Naaim[1]

Received 9 April 2012; revised 14 May 2012; accepted 17 May 2012; published 20 June 2012.

[1] The evaluation of avalanche release depth distributions represents a major challenge for hazard management. This paper presents a rigorous formalism in which these distributions are expressed through a coupling of mechanical and meteorological factors. Considering that an avalanche can occur only if the snowfall depth exceeds a critical value corresponding to a stability criterion, release depth distributions obtained from a slab–weak layer mechanical model are coupled with the distribution of 3-day extreme snowfalls. We show that this coupled model is able to reproduce field data from 369 natural slab avalanches in La Plagne (France). Not only the power-law tail of the distribution, corresponding to large slab depths, but also the core of the distribution for shallow slab depths, are well represented. Small to medium-sized avalanches appear to be controlled mainly by mechanics, whereas large avalanches and the associated power-law exponent, are influenced by a strong mechanical-meteorological coupling. Finally, we demonstrate that the obtained distribution is strongly space-dependent, and, using a consistent interpolation formalism, our model is used to obtain release depth maps for given return periods.
Citation: Gaume, J., G. Chambon, N. Eckert, and M. Naaim (2012), Relative influence of mechanical and meteorological factors on avalanche release depth distributions: An application to French Alps, *Geophys. Res. Lett.*, *39*, L12401, doi:10.1029/2012GL051917.

1. Introduction

[2] The evaluation of avalanche release depth distributions represents a challenging issue for the mapping, zoning and long term management of hazard in mountainous regions. In particular, these distributions constitute one of the essential ingredients (besides friction, terrain, and erosion) to predict accurate run-out distances using avalanche propagation models [*Barbolini et al.*, 2000]. Currently, a strong debate is still ongoing concerning the existence of a possible universal behavior for these distributions. In their pioneering work, *Rosenthal and Elder* [2003] studied a set of 8000 avalanches mixing artificial and natural triggers at Mammoth Mountain (USA), and showed that the release depth cumulative exceedance distribution (CED) appears to follow a power-law of exponent -2.6. This led them to postulate that avalanche release depths are scale-invariant and behave as a chaotic process. They argue that this behavior may be due to the deposition and evolution of snow layers and to the mechanics of slab avalanche release. *McClung* [2003] reported the same behavior and power-law exponent for a set of 187 slab avalanches in British Columbia (mix of triggers), and points out the possible role of fracture toughness distributions and mechanical size effects. This author also analyzed separately artificial and natural avalanche releases to study the effect of the triggering mechanism. A scale-invariant CED tail was also found on the set of 56 natural avalanches, although on a relatively small range of depths in this case and with an apparent power-law exponent of -4.4. *Failletaz et al.* [2006] studied 3450 avalanches in Tignes and La Plagne (France) and also reported a power-law CED with a characteristic exponent of -2.4 for artificially released avalanches. Given the similarity of this result with previous studies carried out in different areas, they concluded on the universality of this power-law exponent. Finally, a more recent study by *Bair et al.* [2008] compares the adjustment of different statistical distributions on release depth data from different mountainous areas, and show that GEV (Generalized Extreme Value) and Frechet distributions seem to provide better fits than power-law distributions for all the analyzed datasets. They also show a significant spatial variation in the power-law exponents of the CED tails and conclude, on the contrary, on a non-universal behavior of avalanche release depth distributions.

[3] In this study, we present a new modeling framework in which the observed avalanche release depth distributions are explained through a coupling of release mechanics and extreme snowfall probabilities. We will show that our approach is capable of satisfactory reproducing release depth data, and supports the conclusions of *Bair et al.* [2008] in that neither the core nor the power-law tail of the CED appear to have universal characteristics.

2. Release Depth Data

[4] Ski patrollers from La Plagne (France) ski resort provided us with a database collecting the release depth of 369 natural and 5323 artificially-triggered slab avalanches that occurred from winters 1998 to 2010. We considered that the typical uncertainty on these data is on the order of 30% (representative error associated to the measurement protocol). Figure 1a shows the obtained release depth CED for both trigger types. In both cases, a power law of exponent α was adjusted to the data for depths higher than a cutoff h_c. As shown in Figure 1b, for artificial releases, the power-law exponent α_a varies only slightly with the chosen cutoff h_c. The best fit, in terms of adjustment error, was found for

[1]IRSTEA, UR ETNA, St Martin d'Heres, France.

Corresponding author: J. Gaume, IRSTEA, UR ETNA, 2 rue de la Papeterie, F-38400 St Martin d'Heres CEDEX, France. (johan.gaume@gmail.com)

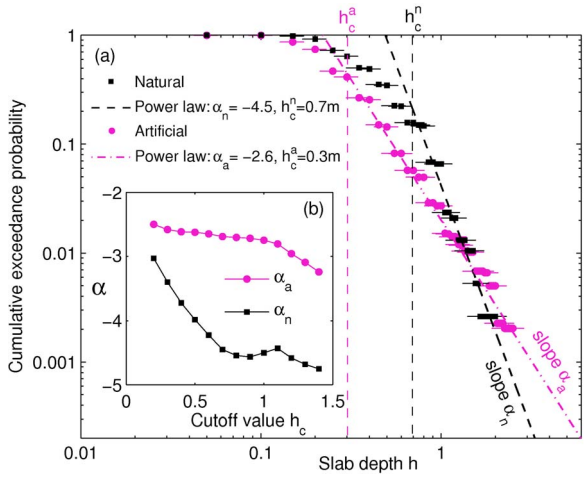

Figure 1. (a) CED of La Plagne slab avalanche release depth data. Natural and artificial avalanches are distinguished and power-laws are adjusted to the tails of the distributions. (b) Power law exponent α as a function of the cutoff value h_c for the two avalanche types.

a relatively low cutoff value h_c^a = 0.3 m and leads to an exponent $\alpha_a = -2.6$, very close to the value reported in previous studies [*Rosenthal and Elder*, 2003; *McClung*, 2003; *Failletaz et al.*, 2006]. On the contrary, for natural releases, the power-law exponent α_n varies significantly with the cutoff h_c, and the power-law regime tends to be restricted to large avalanches only. The best fit, in this case, was found for a cutoff value h_c^n = 0.7 m leading to an exponent $\alpha_n = -4.5$, in agreement with the value reported by *McClung* [2003]. In view of this relatively large cutoff value, however, it is clear that a complete description of the release depth CED cannot be limited to the power-law tail, but needs to encompass the entire depth range. In the following, we focus specifically on the naturally-released slab avalanches, which are generally the most relevant in terms of hazard zoning applications.

3. Coupled Mechanical-Meteorological Model

3.1. Theoretical Framework

[5] Our approach is based on the assumption that a natural slab avalanche occurs when the recent snowfall exceeds a critical depth corresponding to a mechanical stability criterion. In addition, to account for their spatial variability, both the snowfalls and the critical depth are considered in a stochastic framework. Let us thus define $p_m(h)$ and $p_{sf}(h_{sf})$ as the probability densities of the mechanical critical depth h and of the snowfall depth h_{sf}, respectively. Then, the conditional probability density of having an avalanche release depth h knowing that a snowfall of depth h_{sf} occurred, can be expressed as follows:

$$p(h \mid h_{sf}) = \begin{cases} \dfrac{p_m(h)}{\int_0^{h_{sf}} p_m(h')dh'} & \text{if } h \le h_{sf} \\ 0 \text{ if } h > h_{sf} \end{cases}. \quad (1)$$

This amounts to truncating the mechanical distribution $p_m(h)$, retaining only values corresponding to $h \le h_{sf}$ (see Figure 3). Finally the global release depth probability density $p(h)$ is obtained by integrating over all values of h_{sf}:

$$p(h) = \int_0^{\infty} p(h \mid h_{sf}) p_{sf}(h_{sf}) dh_{sf} = p_m(h)\, p_{sf/m}(\ge h), \quad (2)$$

$$\text{where } p_{sf/m}(\ge h) = \int_h^{\infty} \frac{p_{sf}(h_{sf})}{\int_0^{h_{sf}} p_m(h')dh'} dh_{sf}. \quad (3)$$

The avalanche release depth probability is thus expressed through a coupling between mechanical and meteorological factors. As will be shown later, the rigorous coupling equation (2) can be approximated by the following empirical expression:

$$p(h) \approx \tilde{p}(h) = p_m(h) p_{sf}(\ge h)/C, \quad (4)$$

where $p_{sf}(\ge h)$ represents the snowfall CED and $C = \int_0^{\infty} p_m(h')\, p_{sf}(\ge h')dh'$ is a normalization constant. In equation (4), we clearly recognize that the global release depth probability $p(h)$ corresponds to the mechanical probability $p_m(h)$ weighted by the probability of having a snowfall h_{sf} greater than h.

3.2. Mechanical Probability Density $p_m(h)$

[6] To determine the probability density $p_m(h)$ of the critical depth h, a mechanical model of slab avalanche release was built. Such avalanches generally result from the rupture of a weak-layer buried under a cohesive slab [*Schweizer et al.*, 2003, and references therein]. In detail, it has also been shown [*McClung*, 1979; *Schweizer*, 1999] that the shear rupture generally initiates in local weak spots, from which it then propagates through a stress concentration mechanism. The two essential ingredients taken into account in our model are thus the spatial variability of weak-layer mechanical properties and the redistribution of stresses by elasticity of the overlying slab. At this stage, normal collapse of the weak layer, which has been suggested in some studies [*Heierli et al.*, 2008; *van Herwijnen and Heierli*, 2009] to play an important role in the propagation of the instability, is not included.

3.2.1. Formulation of the Model

[7] A 2D (plane stress condition) uniform slope of length L = 50 m, composed of a slab and a weak layer was simulated (Figure 2a) using the finite element code Cast3m. Gravity is the only applied external force and the system is loaded by progressively increasing the slope angle θ until rupture. The slab is elastic with a Young modulus E = 1 MPa, a Poisson ratio ν = 0.2, and a density ρ = 250 kg.m^{-3}. The weak layer is modeled as a quasi-brittle (strain-softening) interface with a Mohr-Coulomb rupture criterion characterized by a cohesion c and a friction coefficient μ = tan 30°. The spatial heterogeneity of the weak layer is represented through a stochastic distribution of the cohesion c which, following *Jamieson and Johnston* [2001] and *Kronholm and Birkeland* [2005], assumes the form a Gaussian law with a spherical covariance function of correlation length ε. An example of an heterogeneity realization for ε = 2 m is represented in Figure 2a. According to *Schweizer et al.* [2008], the values of the correlation length ε have been varied in the range 0.5–10 m. The cohesion standard deviation σ_c was fixed at 0.3 kPa while the average $\langle c \rangle$ was varied in the range 0.6–1.5 kPa,

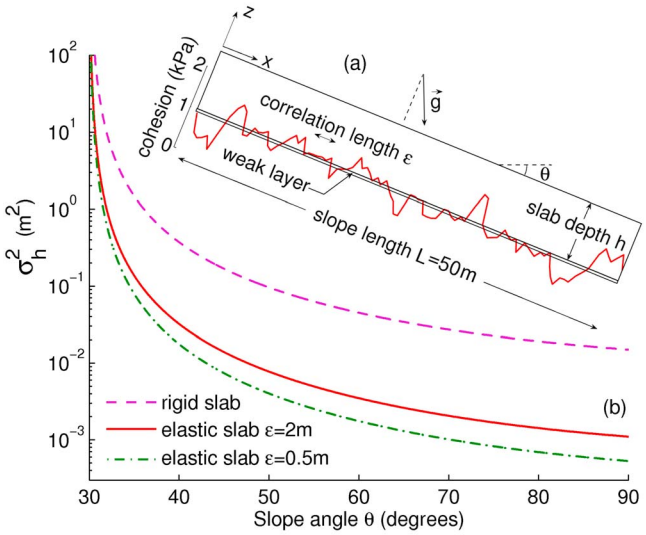

Figure 2. (a) Geometry of the simulated system: a weak layer interface under a cohesive slab of depth h. A realization of the heterogeneity of weak layer cohesion for a correlation length $\varepsilon = 2$ m is represented (average $\langle c \rangle = 1$ kPa, standard deviation $\sigma_c = 0.3$ kPa). (b) Evolution of release depth variance σ_h^2 as a function of slope angle θ for values of correlation length $\varepsilon = 0.5$ m and $\varepsilon = 2$ m. The variance corresponding to a completely rigid slab σ_∞^2 is also shown.

corresponding to coefficients of variation $CV = \sigma_c/\langle c \rangle$ ranging between 20% and 50%.

3.2.2. Release Depth Distributions for a Fixed Slope Angle

[8] More than 5000 simulations were performed for different realizations of the heterogeneity and different sets of model parameters. This allowed us to obtain statistical distributions of release depth h for fixed values of slope angle θ. As a consequence of the Gaussian distribution of the cohesion, these distributions of h are also found to follow Gaussian laws:

$$p(h \mid \theta) = \frac{1}{\sigma_h \sqrt{2\pi}} e^{-\frac{1}{2}\left(\frac{h-\langle h \rangle}{\sigma_h}\right)^2}, \quad (5)$$

where the average $\langle h \rangle$ and the standard deviation σ_h are related to the model parameters as follows: $\langle h \rangle = \langle c \rangle/(\rho g F)$ and $\sigma_h = \sigma_c f(\varepsilon)/(\rho g F) = \sigma_\infty f(\varepsilon)$, with $F = \sin\theta - \mu \cos\theta$, and $f(\varepsilon) \approx \kappa \varepsilon^{1/3}$ ($\kappa = 0.23$ m$^{-1/3}$). The factor σ_∞ represents the standard deviation that would be observed if the stress field in the weak layer exactly followed the heterogeneity variations (case of a completely rigid slab). As shown in Figure 2b, for realistic values of ε, σ_h^2 is always much lower than the rigid slab variance σ_∞^2. In addition σ_h^2 decreases with increasing slope angle θ and with decreasing correlation length ε. These evolutions can be explained by a smoothing effect of the weak-layer heterogeneity due to redistributions of stresses by slab elasticity.

3.2.3. Integration Over All Slope Angles

[9] Since release depth data from La Plagne encompass release zones with various slope angles, the mechanical probability $p_m(h)$ is obtained by integrating the release depth distributions $p(h|\theta)$ derived from mechanical modeling over all values of θ. For the sake of simplicity, we chose to consider a uniform slope probability distribution $p(\theta)$ between $\theta_{\min} = 30°$ and $\theta_{\max} = 90°$. This assumption enables us to obtain an analytical expression for $p_m(h)$:

$$p_m(h) = \int_{\theta_{\min}}^{\theta_{\max}} p(h|\theta) p(\theta) \mathrm{d}\theta = \frac{\sigma_c f(\varepsilon)}{\rho g h^2 \sqrt{2\pi}} [g_1(h) + g_2(h)], \quad (6)$$

with

$$g_1(h) = e^{-\frac{1}{2}U_1^2} - e^{-\frac{1}{2}U_2(h)^2},$$

and

$$g_2(h) = \sqrt{\frac{\pi}{2}} U_1 \left[\mathrm{erf}\left(\frac{U_1}{\sqrt{2}}\right) + \mathrm{erf}\left(\frac{U_2(h)}{\sqrt{2}}\right) \right],$$

where we defined $U_1 = \langle c \rangle/[\sigma_c f(\varepsilon)]$ and $U_2(h) = (\rho g h - \langle c \rangle)/[\sigma_c f(\varepsilon)]$. As shown in Figure 3a, the mechanical probability density $p_m(h)$ displays negligible values below a characteristic depth h_m. This mechanical cutoff results from a combination of the weak-layer Mohr-Coulomb criterion and the slab heterogeneity smoothing effect, and can be approximated as $h_m \approx [\langle c \rangle - 2\sigma_c f(\varepsilon)]/(\rho g)$. A second important observation is that, for $h > h_m$, the CED $p_m(\geq h)$ follows a power-law trend with a characteristic exponent $\Psi_m = -1$ (Figure 4).

3.3. Snowfall Probability Density $p_{sf}(h_{sf})$

[10] Natural avalanches, which generally occur after or during intense precipitations, can be considered as rare

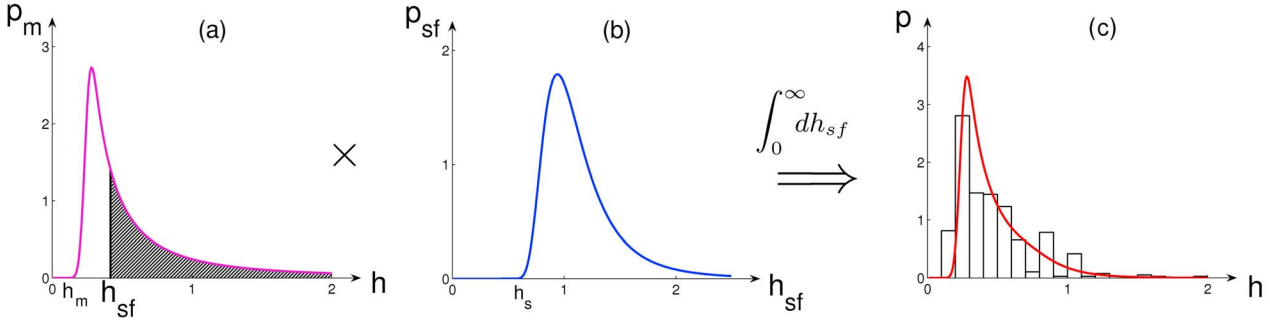

Figure 3. Diagram illustrating the coupling between the mechanical probability p_m and the extreme snowfall probability p_{sf}. (a) Release depth probability density predicted by the mechanical model. The grayed portion corresponds to snow-depth values higher than the available snowfall h_{sf}. (b) Probability density of 3-days extreme snowfalls. (c) Coupled mechanical-meteorological probability density of avalanche release depth. The histogram corresponds to La Plagne data.

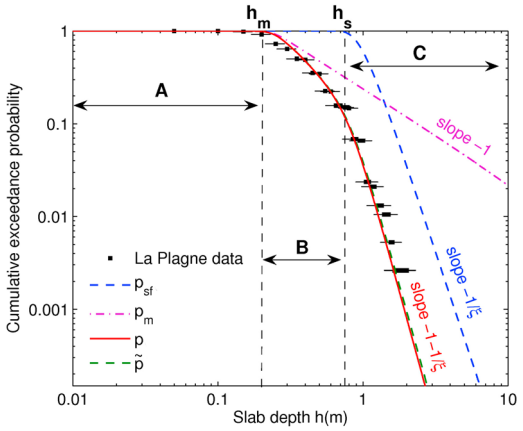

Figure 4. Mechanical release depth CED $p_m(h)$ (equation (6)), extreme snowfall CED $p_{sf}(h)$ (equation (7)), slab release depth CED predicted by the coupled model $p(h)$ (equation (2)), and approximated release depth CED $\tilde{p}(h)$ (equation (4)), compared with field release depth data from La Plagne. The numerical results have been obtained for a correlation length $\varepsilon = 2$ m and an average cohesion $\langle c \rangle = 0.6$ kPa (the other parameters being indicated in text).

events in the statistical sense. In detail, the 3-day extreme snowfall is generally considered as the best avalanche predictor [*Schweizer et al.*, 2003]. Hence, to define the meteorological probability $p_{sf}(h_{sf})$ introduced in equation (2), we analyzed the 3-day snowfall annual maxima in La Plagne (Meteo France data: daily measurements since 1966). These maxima follow a GEV distribution:

$$p_{sf}(\geq h) = 1 - \exp\left[-\left(1 + \xi\frac{h-\mu}{\sigma}\right)^{-1/\xi}\right], \qquad (7)$$

where μ, σ and ξ are, respectively, the location, scale, and shape parameters. Taking moreover into account an average snow density of 60 kg.m^{-3} (24 h-density from La Plagne data) and a settling of the snowpack after 3 days of 30%, meteorological data in water equivalent can be converted into snow heights, which leads to the following GEV parameters: $\mu = 0.98$ m, $\sigma = 0.21$ m and $\xi = 0.214$. As shown in Figure 3b (density) and Figure 4 (CED), the density $p_{sf}(h_{sf})$ is negligible for $h_{sf} < h_s \approx 0.7$ m in La Plagne (in general, h_s is a function of μ, σ and ξ). For $h_{sf} > h_s$, the CED decreases as a power law whose exponent Ψ_{sf} is directly related to the shape parameter ξ of the GEV: $\Psi_{sf} = -1/\xi \approx -4.68$ in La Plagne. Note that the existence of this power-law tail comes from the fact that the GEV in La Plagne belongs to the Fréchet domain ($\xi > 0$). It would not be the case with Weibull ($\xi < 0$) or Gumbel ($\xi = 0$) distributions.

3.4. Coupling Result

[11] The coupled release depth probability $p(h)$ computed from equation (2) is represented on Figure 3c (density) and Figure 4 (CED). First, it can be noted that, as already mentioned, the approximate probability $\tilde{p}(h)$ (equation (4)) is almost identical to the rigorous coupled probability $p(h)$ for the whole range of depths considered. Concerning the shape of $p(h)$, three different zones can be distinguished (Figure 4). In zone A, for $h < h_m$ no avalanche can occur. Hence, a new snowfall has to be larger than h_m, after settling, to potentially trigger an avalanche. In zone B, corresponding to $h_m \leq h \leq h_s$ (small to medium-sized avalanches), the coupled CED shows a concave shape (in log-log scales). This zone corresponds to a regime of weak coupling in which the release depth probability $p(h)$ is essentially controlled by the mechanical probability $p_m(h)$, the available amount of snow being always sufficient to trigger an avalanche if the mechanical criterion is reached. Lastly, zone C for $h > h_s$ (large avalanches) corresponds to a regime of strong coupling. Snowfall depths larger than h_s become infrequent and thus play the role of a limiting factor on the mechanical probability $p_m(h)$ in the expression of the coupled probability $p(h)$. In this regime, as a direct consequence of the power-law trends displayed both by $p_m(h)$ and $p_{sf}(h)$, the coupled release depth CED also decreases as a power-law. According to equation (4), the corresponding exponent is equal to $\Psi = \Psi_m + \Psi_{sf} = -1 - 1/\xi$.

4. Comparison With Data and Discussion

[12] As shown in Figures 3 and 4, the coupled model presented above is able to reproduce La Plagne data with excellent accuracy. Both the power-law tail, corresponding to large slab depths, and the core of the distribution for shallow slab depths, are well represented. To obtain this result, only the mechanical cutoff h_m was adjusted, which in turn depends on a combination of the average cohesion $\langle c \rangle$, the slab density ρ, the cohesion standard deviation σ_c and the heterogeneity correlation length ε. In our case, the best agreement with the data was obtained for a value $h_m \approx 0.18$ m, which corresponds for instance to $\langle c \rangle = 0.6$ kPa and $\varepsilon = 2$ m (the other parameters being fixed as indicated in Section 3.2). Note also that the obtained agreement critically depends on the fact that, for values of ε in the meter range, the variance σ_h^2 of the mechanical distribution $p_m(h)$ is relatively low due to the elastic smoothing effect (Figure 2b). A less satisfactory data adjustment in zone B would be obtained with values of ε larger than 10–15 m.

[13] Concerning the power-law tail of the CED, it can be noted that, in spite of the good agreement observed in Figure 4, the exponent value $\Psi \approx -5.68$ predicted by the model is lower than $\alpha_n \approx -4.5$ estimated directly from release depth data. This highlights the difficulty of accurately assessing a power-law exponent on the few data corresponding to large avalanches, as already pointed out by *McClung* [2003]. An important outcome of our coupled model is that the tail exponent Ψ strongly depends on the local meteorological conditions through the shape parameter ξ of the GEV distribution of extreme snowfalls. In the French Alps, ξ-values are generally positive, but present an important spatial variability at regional scale, typically varying between -0.2 and 0.4. Hence, in agreement with the conclusions of *Bair et al.* [2008], the decay of the tail of natural slab avalanche release depth CED cannot be expected to be universal.

[14] More generally, due to the spatial heterogeneity of the GEV parameters and mechanical properties, it is actually the complete distribution of avalanche release depths which is strongly variable from one location to another. To highlight this point, our model has been used to predict avalanche release depths for a given return period over all French Alps. For that purpose, a spatial interpolation of 3-day extreme snowfall data has been performed using a robust mathematical formalism based on Max-Stable processes and properly

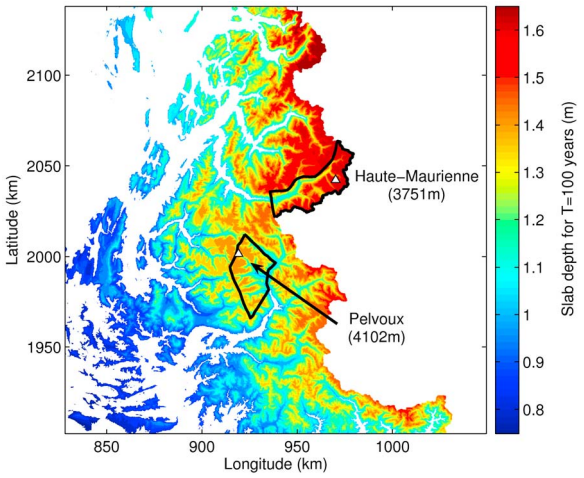

Figure 5. Map of slab avalanche release depth in the French Alps for a return period of 100 years and elevations higher than 1000 m.

accounting for the spatial dependence of the data [*Blanchet and Lehning*, 2010; *Blanchet and Davison*, 2011]. A brief description of this spatial model can be found in *Eckert et al.* [2010, 2011]. As shown in Figure 5, the results highlights that, at first order, avalanche release depths are dominated by altitudinal effects. However, in detail, the variation patterns of the GEV parameters with latitude and longitude can also be noticed. For instance, the release depths predicted in the Haute-Maurienne massif culminating at 3751 m are significantly higher (>1.6 m) than those in the Pelvoux massif culminating at 4102 m (<1.4 m). Note that, at this stage, these spatial trends are purely due to snowfall properties since the values of all mechanical parameters have been assumed constant in this interpolation. In a further step, spatialization of the cohesion distributions will also need to be considered, but additional data will be required for that purpose.

5. Conclusion

[15] This paper investigates the relative influence of mechanical and meteorological factors on avalanches release depth distributions. A robust formalism for the coupling of a stochastic stability criterion (resulting from spatial heterogeneity of the mechanical properties) with extreme snowfall distributions has been developed. It has been shown that this coupled mechanical-meteorological model is able to reproduce with excellent accuracy the release depth distribution corresponding to 369 natural slab avalanches in La Plagne (France). Not only the power-law tail, corresponding to large slab depths, but also the core of the distribution for shallow slab depths, are well represented. This agreement does not prove that the physical mechanisms of avalanche release are fully captured in the model proposed. However, the retained ingredients appear sufficient to produce realistic release depth distributions and to provide an interpretation of the distribution parameters (cutoff, exponent, etc.) in terms of clearly-identified nivological properties.

[16] From the model, three avalanche release regimes have been identified. Large avalanches, in particular, are controlled by a strong coupling between mechanical and meteorological factors. In agreement with previous studies, the release depth CED in this regime behaves as a power-law. However, the corresponding exponent directly depends on the shape parameter of the meteorological GEV distribution and, thus, cannot be considered as universal.

[17] From an operational perspective, the model presented in this paper can be viewed as a powerful tool capable of evaluating avalanche depth distributions at any location, provided snowfall data are available or a suitable spatial interpolation procedure is used. It can be highlighted that, compared to the classical engineering method in which only the 3-day extreme snowfalls are taken into account, the release depth values for a given return period computed with our coupled model generally tend to be lower (see Figure 4).

[18] **Acknowledgments.** Support from the European Interreg DYNAVAL and the ANR MOPERA projects is acknowledged. We also wish to express our gratitude to C. Schneider, snow expert in La Plagne, for providing release depth data and to the two reviewers, M. Lehning and J. Schweizer, for their insightful and constructive comments. Support from the European Interreg DYNAVAL and MAP3 projects and from the ANR MOPERA is acknowledged.

[19] The Editor thanks Michael Lehning for assisting in the evaluation of this paper.

References

Bair, E. H., J. Dozier, and K. W. Birkeland (2008), Avalanche crown-depth distributions, *Geophys. Res. Lett.*, *35*, L23502, doi:10.1029/2008GL035788.

Barbolini, M., U. Gruber, C. Keylock, M. Naaim, and F. Savi (2000), Application and evaluation of statistical and hydraulic-continuum dense-snow avalanche models to five real European sites, *Cold Reg. Sci. Technol.*, *31*(2), 133–149.

Blanchet, J., and A. Davison (2011), Spatial modelling of extreme snow depth, *Ann. Appl. Stat.*, *5*(3), 1699–1725.

Blanchet, J., and M. Lehning (2010), Mapping snow depth return levels: Smooth spatial modeling versus station interpolation, *Hydrol. Earth Syst. Sci. Discuss.*, *7*, 6129–6177.

Eckert, N., C. Coleou, H. Castebrunet, M. Deschatres, D. Giraud, and J. Gaume (2010), Cross-comparison of meteorological and avalanche data for characterising avalanche cycles: The example of December 2008 in the eastern part of the French Alps, *Cold Reg. Sci. Technol.*, *64*, 119–136.

Eckert, N., J. Gaume, and H. Castebrunet (2011), Using spatial and spatial-extremes to characterize snow avalanche cycles, *Procedia Environ. Sci.*, *7*, 224–229.

Failletaz, J., F. Louchet, and J. Grasso (2006), Cellular automaton modelling of slab avalanche triggering mechanisms: From the universal statistical behaviour to particular cases, in *Proceedings of the ISSW 2006*, pp. 174–180, Int. Snow Sci. Workshop, Telluride, Colo.

Heierli, J., P. Gumbsch, and M. Zaiser (2008), Anticrack nucleation as triggering mechanism for snow slab avalanches, *Science*, *321*, 240–243.

Jamieson, J., and C. Johnston (2001), Evaluation of the shear frame test for weak snowpack layers, *Ann. Glaciol.*, *32*, 59–69.

Kronholm, K., and K. W. Birkeland (2005), Integrating spatial patterns into a snow avalanche cellular automata model, *Geophys. Res. Lett.*, *32*, L19504, doi:10.1029/2005GL024373.

McClung, D. M. (1979), Shear fracture precipitated by strain softening as a mechanism of dry slab avalanche release, *J. Geophys. Res.*, *84*(B7), 3519–3526, doi:10.1029/JB084iB07p03519.

McClung, D. M. (2003), Size scaling for dry snow slab release, *J. Geophys. Res.*, *108*(B10), 2465, doi:10.1029/2002JB002298.

Rosenthal, W., and K. Elder (2003), Evidence of chaos in slab avalanching, *Cold Reg. Sci. Technol.*, *37*, 243–253.

Schweizer, J. (1999), Review of dry snow slab avalanche release, *Cold Reg. Sci. Technol.*, *30*, 43–57.

Schweizer, J., J. Bruce Jamieson, and M. Schneebeli (2003), Snow avalanche formation, *Rev. Geophys.*, *41*(4), 1016, doi:10.1029/2002RG000123.

Schweizer, J., K. Kronholm, J. Jamieson, and K. Birkeland (2008), Review of spatial variability of snowpack properties and its importance for avalanche formation, *Cold Reg. Sci. Technol.*, *51*(*2–3*), 253–272.

van Herwijnen, A., and J. Heierli (2009), Measurement of crack-face friction in collapsed weak snow layers, *Geophys. Res. Lett.*, *36*, L23502, doi:10.1029/2009GL040389.